

On Diffusion-Induced Non-Constant Composition Profiles in the Boundary Layer of Inert Multicomponent Mixtures

Sverre Gullikstad Johnsen^{1,2†}

¹SINTEF Industry, Trondheim, Norway

²NTNU, dept. Materials Science and Engineering, Trondheim, Norway

(Received xx; revised xx; accepted xx)

In the boundary layer of multicomponent fluid mixtures, the species-specific mass flux in the wall-normal direction is determined by the combination of turbulent-diffusiophoretic diffusion due to composition gradients, and diffusion due to gradients in other scalar fields (e.g. thermophoresis, barophoresis, and forced diffusion). For inert mixtures, a balance must exist between all the diffusive transport mechanisms so that the net diffusive mass flux normal to the wall is zero everywhere. This paper discusses under which conditions non-constant composition profiles are necessary to obtain physico-chemical equilibrium, hence vanishing transport, in the wall-normal direction.

Mathematical modeling is employed to demonstrate how this may affect fluid property profiles, wall heat flux, and wall shear stress in an ideal, ternary gas mixture ($H_2 + N_2 + CO_2$) subject to a temperature gradient.

It is concluded that competing diffusive transport mechanisms, under certain circumstances, may result in non-constant composition profiles and significantly different wall and bulk compositions, for inert multicomponent mixtures. Hence, wall-normal diffusion in the boundary layer must be accounted for to correctly describe or interpret multicomponent flow systems sensitive to wall friction and heat exchange.

1. Introduction

The classical experiment by Duncan & Toor (1962) showed that the diffusive transport in an ideal ternary gas mixture of hydrogen (H_2), nitrogen (N_2), and carbon dioxide (CO_2) could not be described satisfactorily by Fickian diffusion theory. E.g., the observed development in local nitrogen concentrations could only be explained mathematically by allowing uphill diffusion. The Duncan-Toor experiments have been further investigated and discussed by e.g. Taylor & Krishna (1993) and Krishna & Wesselingh (1997). It has been shown that Maxwell-Stefan diffusion theory predicts the non-Fickian behavior observed by Duncan and Toor, accurately.

Whereas the Duncan-Toor experiments were performed under isothermal conditions, Bogatyrev *et al.* (2015) studied thermophoresis in binary, ternary, and quaternary mixtures including the ternary $H_2 - N_2 - CO_2$ mixture. They emphasized that thermophoresis in multicomponent mixtures depends on the mixture composition in a complex way.

Gibbs (1928) was the first to suggest a formula for calculating compositional variations due to gravity, based on vanishing gradients in the physico-chemical potential. Later, significant compositional gradients observed in subsurface oil/gas reservoirs have been credited gravity-chemical equilibrium, e.g. in the Brent field in the North Sea (Schulte

† Email address for correspondence: sverregu@gmail.com

1980). Moreover, it is well known that centrifugal forces can induce species segregation (Svedberg 1927). This phenomenon has widespread industrial and scientific application in e.g. materials science, chemistry, and biotechnology.

Physico-chemical equilibrium demands zero net wall-normal transport for each species, everywhere in the boundary layer of inert mixtures. It is evident, however, that competing diffusive processes which cancel each other out, can fulfill this requirement. Hence, it is suggested that under certain conditions, non-constant composition profiles in the wall-normal direction may result from non-Fickian behavior.

Such spatial composition variations will affect fluid properties (e.g. mass density, viscosity, and thermal conductivity) hence the wall heat flux and wall shear stress. Thus, without the proper understanding, interpretation of e.g. rheology measurements may fail to give a correct assessment of the fluid properties, even for the simplest multicomponent mixtures. This paper discusses, with basis in Maxwell-Stefan diffusion theory, under which conditions non-constant composition profiles in the boundary layer must be accounted for. It is shown, by computational example, how this can impact the estimated wall heat flux and wall shear stress.

Using the ideal ternary gas mixture of Duncan & Toor (1962) as an example, mathematical modeling is employed to demonstrate how a compositional gradient must be present to balance the temperature gradient, to achieve zero net mass flux. Comparing simulations with and without diffusion, the expected consequences of the diffusion-induced, non-constant composition profiles on wall heat flux and wall shear stress is estimated.

2. Mathematical models

We are considering a single-phase fluid mixture consisting of a set of N unique, distinguishable, inert species. It is assumed that each species field, hence the fluid itself, can be modeled as a continuum. This implies that molecular scale effects are neglected, and species and fluid properties are well defined, continuously varying physical fields throughout the fluid domain. Furthermore, it is assumed homogeneous mixing in the sense that local species properties are taken as volume averages over infinitesimal volumes. These assumptions allow the utilization of differential calculus in deriving local governing equations for the species transport. For a discussion of fluid dynamics at length scales below the thermodynamic limit, see e.g. (Dyson & Ransing 2005; Dyson *et al.* 2008).

2.1. Governing Equations

The set of steady-state governing equations consists of the Advection-Diffusion equation for each species, the fluid mixture momentum and energy equations, and the restriction that the mass- and mole-fractions must sum to unity:

$$\nabla \cdot (\rho_f x_i \mathbf{u}_f) + \nabla \cdot \mathbf{j}_{d,i} = 0 ; \quad (2.1)$$

$$\nabla \cdot (\rho_f \mathbf{u}_f \mathbf{u}_f) = -\nabla P + \nabla \cdot \boldsymbol{\tau} + \rho_f \mathbf{f} ; \quad (2.2)$$

$$\nabla \cdot (\rho_f h_{sens,f} \mathbf{u}_f) = \nabla \cdot (k_f \nabla T) - \nabla \cdot \left(\sum_{i=1}^N \mathbf{j}_{d,i} h_{sens,i} \right) ; \quad (2.3)$$

$$\sum_{i=1}^N x_i = \sum_{i=1}^N z_i = 1 . \quad (2.4)$$

ρ_f and k_f are the mass density and thermal conductivity of the fluid, respectively, x_i and z_i are the mass and mole-fractions of species i , respectively, and \mathbf{u}_f is the mass-averaged

advective fluid velocity vector. The diffusive mass flux is defined as the difference between the convective and advective mass fluxes,

$$\mathbf{j}_{d,i} \equiv \rho_i (\mathbf{u}_i - \mathbf{u}_f) , \quad (2.5)$$

where ρ_i and \mathbf{u}_i are the mass concentration and convective velocity vector of species i , respectively. P and T are pressure and temperature, respectively, τ is the shear stress tensor, \mathbf{f} is the net specific body force vector, and $h_{sens,i}$ is the specific sensible enthalpy of species i .

Introducing turbulence, dimensionless variables marked with superscript $+$ (see Appendix), and appropriate simplifications in the near-wall region, the simplified governing equations are obtained:

$$(\nu_t^+ \rho_f^+ / Sc_t) \partial_{\perp} x_i - j_{d,i,\perp}^+ = 0 ; \quad (2.6)$$

$$\rho_f^+ \partial_{\perp} u_{f,\parallel}^+ = 1 / (\nu_f^+ + \nu_t^+) ; \quad (2.7)$$

$$\partial_{\perp} \left[k_t^+ \left(\partial_{\perp} \ln c_{P,f}^+ \right) T^+ + \left(k_f^+ + k_t^+ \right) \partial_{\perp} T^+ \right] = 0 . \quad (2.8)$$

The \perp and \parallel indicate the directions normal to the wall and parallel with the wall and bulk flow direction, respectively, and ∂_{\perp} denotes the dimensionless gradient component in the direction perpendicular to the wall. Sc_t denotes the turbulent Schmidt number, ν_f and ν_t are the fluid and turbulent kinematic viscosities, respectively, k_t is the turbulent thermal conductivity, and $c_{P,f}$ is the fluid specific heat capacity. It is noted that equations 2.6-2.8 are valid in the laminar limit where $\nu_t^+ / Sc_t \rightarrow 0$, $\nu_t^+ \rightarrow 0$, and $k_t^+ \rightarrow 0$. For more details, refer to Johnsen *et al.* (2015).

2.2. Diffusion flux

Assuming local equilibrium (see Kjelstrup & Bedeaux 2008, Ch. 3.5), local entropy production due to fluid species migration must be positive. Hence, diffusion acts to minimize the physico-chemical potential of the fluid. Following de Groot & Mazur (2011), the gradient of the dimensionless physico-chemical potential of species j is expressed as $\nabla \psi_j^+ = \nabla \mu_j^+ - (M_{m,j} / RT) \mathbf{f}_j$, where $\mu_j^+ = \mu_j^{0+}(T, P) + \ln(\gamma_j z_j)$, γ_j , and $M_{m,j}$ are the dimensionless chemical potential, activity coefficient, and molar mass of species j , respectively, R is the universal gas constant, and \mathbf{f}_j is the net conservative specific external body force acting on species j (e.g. gravitational, centrifugal, and electromagnetic forces per unit mass). The diffusion mass flux is expressed as a resultant of the scaled, negative physico-chemical potential gradients of all the species in the fluid mixture;

$$j_{d,i,\perp}^+ = -\rho_f^+ D_{ij}^+ \partial_{\perp} \psi_j^+ , \quad (2.9)$$

where Einstein summation is employed and D_{ij} is the multicomponent diffusion coefficient of species i in species j . It follows from Eq. (2.5) that the diffusive mass fluxes sum to zero, and by combining Eqs. (2.6) and (2.9), it is seen that zero net mass transport can only be ensured by requiring that the diffusion flux is balanced by turbulent diffusion;

$$D_{ij}^+ \partial_{\perp} \psi_j^+ = -(\nu_t^+ / Sc_t) \partial_{\perp} x_i . \quad (2.10)$$

Mechanical equilibrium is assumed throughout the paper. Eq. (2.2) then reduces to $\nabla P = -\rho_f \sum_{i=0}^N x_i \mathbf{f}_i$, where it has been assumed that the total, specific, external body force acting on the fluid can be decomposed into species-specific components, \mathbf{f}_i . Expanding the chemical potential gradient in its partial derivatives, Eq. (2.9) may now

be written as (Taylor & Krishna 1993; Kocherginsky & Gruebele 2016)

$$j_{d,i,\perp}^+ = -\rho_f^+ D_{ij}^+ \left[\Gamma_{jk} \Lambda_{kl} \partial_{\perp} x_l + d_{T,j} \partial_{\perp} \ln(T^+ + T_{wall}^{0+}) \right. \\ \left. + \frac{1}{RT} \left(V_{m,j} - \frac{M_{m,j}}{\rho_f} \right) \partial_{\perp} P - \frac{1}{RT} \frac{\nu_{f,wall}}{u_{\tau}} \left(F_{j,\perp} - M_{m,j} \sum_{k=1}^N x_k f_{k,\perp} \right) \right], \quad (2.11)$$

where the diffusiphoretic and thermophoretic driving force coefficients are defined as $\Gamma_{jk} = \partial \mu_j^+ / \partial z_k$ and $d_{T,j} = \partial \mu_j^+ / \partial \ln(T^+ + T_{wall}^{0+})$, respectively, $\Lambda_{kl} \partial_{\perp} X_l = \partial_{\perp} z_k$, the subscript *wall* indicates property values at the wall, V_m is the molar volume, u_{τ} is the shear velocity, $F_{j,\perp} = M_{m,j} f_{j,\perp}$ (summation not intended) is the molar body force acting on species j in the wall-normal direction, and it is implicitly understood that partial derivatives are taken with respect to one variable while keeping all other variables constant. Hence, the diffusion flux can be decomposed into a diffusiphoretic term due to composition gradients, a thermophoretic term due to temperature gradients, a barophoretic term due to pressure gradients, and a forced diffusion term due to external forces. It is noted that $\partial_{\perp} P = 0$ if $\sum_{k=1}^N x_k f_{k,\perp} = 0$.

3. How can Non-Constant Composition Profiles Occur in the Boundary Layer?

Based on the governing equations and relations described in the previous section, this section discusses the mathematical requirements for obtaining non-constant composition profiles in the boundary-layer. Three main regimes are discussed:

- (i) Isothermal conditions in the absence of body forces.
- (ii) Non-isothermal conditions in the absence of body forces.
- (iii) Isothermal conditions under influence of body forces (gravitational/centrifugal).

The discussion is of a general nature, and it is shown how all three scenarios allow (at least mathematically), or even demand the generation of non-constant composition profiles. Due to the additive nature of the diffusive driving forces, the scenarios discussed cover most situations that can occur. Body forces due to electromagnetic forces on charged or polarized species has not been discussed due to the difficulties associated with drawing general conclusions regarding the resulting composition profiles. This difficulty is due to the multitude of different situations that can arise depending on the electric charge of the species. For instance, in a given circumstance, the mass averaged electrostatic body force can be zero, causing the pressure gradient to vanish. Replacing one of the species with another species of different electric charge, will change this, producing a non-zero pressure gradient. Moreover, separation of electrically charged species will cause deviation from quasi neutrality of the fluid. Hence, the Poisson equation, for the electrostatic field, must be added to the set of governing equations to calculate local electrostatic field strengths. Furthermore, electrically charged species tend to be reactive, not inert. This paper discusses inert fluids, only. That being said, there is no doubt, however, that electromagnetic forces, similar to gravitational/centrifugal forces, can be the source of species separation.

3.1. Isothermal conditions in the absence of body forces

Eq. (2.6) can be written as a homogeneous system of equations:

$$D_{X,il}^+ \partial_{\perp} x_l = 0, \quad (3.1)$$

where $D_{X,il}^+ = [(\nu_i^+/s_{c_i}) \delta_{il} + D_{ij}^+ \Gamma_{jk} \Lambda_{kl}]$ and δ_{il} is the Kronecker delta. Eq. (3.1) has a non-trivial solution ($\partial_\perp x_l \neq 0$) if and only if $-\nu_i^+/s_{c_i}$ is a non-zero eigenvalue of the matrix product $\mathbf{D}^+ \Gamma \Lambda$. Mathematically this is permitted, but it would be an absolutely remarkable coincidence if this was to be true for all wall distances in a physical boundary layer. Hence, it can be deduced that it is very unlikely that a non-constant composition profile can develop in the absence of temperature gradients and/or body forces. It is noted that at the wall, where $\nu_i^+/s_{c_i} \rightarrow 0$, the required condition for a non-trivial solution reduces to $\det(\Gamma) = 0$, since both \mathbf{D}^+ and Λ are invertible. In particular, this is impossible for ideal mixtures ($\gamma_j = 1 \forall j$), since Γ becomes diagonal with non-zero elements, only.

3.2. Non-isothermal conditions in the absence of body forces

In the presence of non-zero temperature derivatives in the wall-normal direction, there must be a balance between the turbulent-diffusiophoretic diffusion on one side and thermophoretic diffusion on the other. This balance can be formulated as the non-homogeneous system of equations

$$D_{X,il}^+ \partial_\perp x_l = -D_{ij}^+ d_{T,j} \partial_\perp \ln(T^+ + T_{wall}^{0+}) . \quad (3.2)$$

It is evident that non-zero mass-fraction gradients are required to counter the thermophoresis, in general. At the wall, Eq. (3.2) reduces to

$$\Gamma_{jk} \partial_\perp z_k|_{wall} = -d_{T,j,wall} Pr_{wall}/T_{wall}^{0+} , \quad (3.3)$$

which in combination with Eq. (2.4) produces the requirement that $\sum_{j=1}^N z_j d_{T,j} = 0$ holds at the wall, for ideal mixtures. This implies that d_T components of both positive and negative values must exist at the wall, for ideal mixtures.

3.3. Isothermal conditions under influence of body forces

In the presence of external body forces in the wall-normal direction, there must be a balance between the turbulent-diffusiophoretic, barophoretic, and forced diffusion. From Eqs. 2.6 and 2.11, we have

$$D_{X,il}^+ \partial_\perp x_l = -\frac{1}{RT} D_{ij}^+ \left[\left(V_{m,j} - \frac{M_{m,j}}{\rho_f} \right) \partial_\perp P - \frac{\nu_{f,wall}}{u_\tau} \left(F_{j,\perp} - M_{m,j} \sum_{k=1}^N x_k f_{k,\perp} \right) \right] . \quad (3.4)$$

If the body forces are due to gravity or centrifugal forces, the forced diffusion term cancels out due to the non-discriminating effect on the various species, $f_{j,\perp} \equiv f_\perp$, where

$$f_\perp = \begin{cases} g_\perp & \text{for gravitational body force,} \\ \omega^2 r_\perp & \text{for centrifugal body force,} \end{cases} \quad (3.5)$$

where r_\perp is the wall-normal distance from the center of rotation. Eq. (3.4) thus reduces to the non-homogeneous system of equations

$$D_{X,il}^+ \partial_\perp x_l = D_{ij}^+ \left[\frac{\nu_{f,wall}}{u_\tau} \frac{f_\perp M_{m,j}}{RT} \left(1 - \frac{\rho_f}{\rho_j^0} \right) \right] , \quad (3.6)$$

where $\rho_j^0 = M_{m,j}/V_{m,j}$ denotes the mass density of the pure species, j , and summation over the repeated j index inside the square brackets is not intended. If the mass density of the pure species differs from that of the fluid mixture, it is evident that non-constant composition profiles are required to counter the effect of the forced diffusion.

For an ideal mixture of perfect gases in the absence of turbulence ($\nu_i^+/s_{c_i} = 0$

| | Lennard-Jones param. | | | |
|--------|----------------------|----------|-------|------------|
| | M_m | c_p^1 | d | Ω^1 |
| | [kg/mol] | [J/molK] | [Å] | [-] |
| H_2 | 0.002016 | 28.84 | 2.915 | 0.857 |
| N_2 | 0.02801 | 29.12 | 3.681 | 1.022 |
| CO_2 | 0.04401 | 37.12 | 3.996 | 1.296 |

¹ values at 298K.

TABLE 1. Species specific properties.

everywhere), two special cases are emphasized, namely 1) dilute mixture, and 2) binary mixture. For a mixture dilute in species i , $1 - z_i \approx 1$, and the solution to Eq. (3.6) becomes

$$z_i = z_{i,bulk} \exp \left[-\frac{\nu_{f,wall}}{u_\tau} \frac{f_\perp (M_{m,i} - \bar{M}_{m,i}^*)}{RT} (y_{bulk}^+ - y^+) \right], \quad (3.7)$$

where subscript *bulk* indicates property values at a reference point at the outskirts of the boundary layer, $\bar{M}_{m,i}^* \equiv \frac{1}{(1-z_i)} \sum_{\substack{j=1 \\ j \neq i}}^N M_{m,j} z_j$, it was assumed that f_\perp is approximately constant throughout the boundary layer, and y^+ is the dimensionless distance to the wall. Similarly, for a binary mixture, it can be shown that the ratio between the mole-fractions of the two species is given by

$$\left(\frac{z_1}{z_2} \right) = \left(\frac{z_{1,bulk}}{z_{2,bulk}} \right) \exp \left[-\frac{\nu_{f,wall}}{u_\tau} \frac{f_\perp (M_{m,1} - M_{m,2})}{RT} (y_{bulk}^+ - y^+) \right]. \quad (3.8)$$

In both cases, segregation is governed by the dimensionless group $\frac{\nu_{f,wall}}{u_\tau} \frac{f_\perp \Delta M_m}{RT}$, where ΔM_m denotes the difference between the species' molar mass and the representative molar mass of the other species. In particular, $\left| \frac{RT}{f_\perp \Delta M_m} \right|$ is the segregation length. For the segregation length to be of the same order of magnitude as the boundary layer thickness, a large f_\perp is generally required, many orders of magnitude larger than the gravitational force. The effect of turbulence will be to reduce the magnitude of the composition derivatives, since it contributes with a positive addition in $D_{X,il}^+$ on the left hand side of Eq. (3.6). Hence, the effect of turbulence will be reduced segregation efficiency.

4. Ternary Ideal Mixture - Computed example

4.1. Model fluid

The model fluid is a ternary, calorically perfect mixture of perfect gases consisting of 50, 25, and 25 mass-% of H_2 , N_2 , and CO_2 , respectively. Species specific heat capacities were extracted from (Linstrom & Mallard 2018) while species specific viscosities and thermal conductivities were calculated based on Lennard-Jones parameters found in (Anderson 2006). Details regarding the modeling of species and mixture material properties (mass density, viscosity, etc.) can be found in (Johnsen *et al.* 2015). Species specific input data are summarized in table (1).

For a ternary mixture, there are two independent mass-fraction equations in addition to the velocity and temperature equations. Moreover, there are only two independent diffusive mass-fluxes, and the matrices that take part in Eq. (2.11) are 2×2 matrices.

| | |
|--------------|---|
| $H_2 - N_2$ | $D_{12} = 8.33 \cdot 10^{-5} \text{m}^2/\text{s}$ |
| $H_2 - CO_2$ | $D_{13} = 6.80 \cdot 10^{-5} \text{m}^2/\text{s}$ |
| $N_2 - CO_2$ | $D_{23} = 1.68 \cdot 10^{-5} \text{m}^2/\text{s}$ |

TABLE 2. Binary Maxwell-Stefan diffusion coefficients for the ternary $H_2 - N_2 - CO_2$ mixture (Duncan & Toor 1962).

| j | α_{T,j,H_2} | α_{T,j,N_2} | α_{T,j,CO_2} | $d_{T,j}$ |
|-------|--------------------|--------------------|---------------------|-----------|
| H_2 | | 0.32 | 0.38 | 0.161 |
| N_2 | 0.24 | | 0.06 | 0.073 |

TABLE 3. Thermal diffusion factors, $\alpha_{T,jl}$, based on data from (Bogatyrev *et al.* 2015) and resulting thermophoretic driving force coefficients, $d_{T,j}$ (assuming ideal mixture, see Eq. (4.4)).

The elements of the diffusivity matrix, \mathbf{D} , can be expressed as (Taylor & Krishna 1993)

$$\begin{aligned}
 D_{11} &= D_{13}[z_1 D_{23} + (1-z_1) D_{12}] / S, \\
 D_{12} &= z_1 D_{23} [D_{13} - D_{12}] / S, \\
 D_{21} &= z_2 D_{13} [D_{23} - D_{12}] / S, \\
 D_{22} &= D_{23} [z_2 D_{13} + (1-z_2) D_{12}] / S,
 \end{aligned} \tag{4.1}$$

where $S = z_1 D_{23} + z_2 D_{13} + z_3 D_{12}$, the D_{ij} are the binary Maxwell-Stefan diffusion coefficients, and the indexes 1, 2 and 3 relate to H_2 , N_2 , and CO_2 , respectively. The binary Maxwell-Stefan diffusivities employed by Duncan & Toor (1962) are cited in table (2). It is noted that the Onsager reciprocal relation implies that $D_{ij} = D_{ji}$ (Hirschfelder *et al.* 1964; Muckenfuss 1973).

Bogatyrev *et al.* (2015) reported thermal diffusion factors, α_T , as functions of composition for each of the mixture species. The thermal diffusion factors are related to the diffusiophoretic driving force coefficients, $d_{T,j}$ via the thermal diffusion ratio, $k_{T,k}$, by (see van der Valk 1963)

$$d_{T,j} = \Gamma_{jk} k_{T,k}, \tag{4.2}$$

where

$$k_{T,k} = z_k \sum_{\substack{l=1 \\ l \neq k}}^N z_l \alpha_{T,kl}. \tag{4.3}$$

For ideal mixtures, Eq. (4.2) reduces to

$$d_{T,j} = \sum_{\substack{l=1 \\ l \neq j}}^N z_l \alpha_{T,jl}. \tag{4.4}$$

Using the experimental data points at $z_l \approx 0.5$ from Bogatyrev *et al.* (2015), the thermal diffusion factors and thermophoretic driving force coefficients given in table (3) were obtained. For simplicity, constant $d_{T,j}$ were employed in the simulations.

| Boundary Condition | Variable | Value | Unit |
|--------------------------|------------------------|----------|---------------------|
| bulk mass-fractions | $X_{H_2,bulk}$ | 0.5 | kg/kg |
| | $X_{N_2,bulk}$ | 0.25 | kg/kg |
| wall diffusion mass flux | $j_{d,H_2,\perp,wall}$ | 0 | kg/m ² s |
| | $j_{d,N_2,\perp,wall}$ | 0 | kg/m ² s |
| bulk temperature | T_{bulk} | 800 | K |
| wall temperature | T_{wall} | 280 | K |
| bulk flow velocity | $u_{f,\parallel,bulk}$ | 1,2,5,10 | m/s |

TABLE 4. Boundary conditions employed in simulations.

4.2. Simulation setup

The equations were solved in a numerical modeling framework described by Johnsen *et al.* (2015). The simulations assume fully developed turbulent flow parallel to the wall. Moreover, it is assumed that gradients in the main flow direction are negligible and that gradients perpendicular to the wall vanish in the bulk. Additional details can be found in (Johnsen *et al.* 2015).

The wall and bulk temperatures were set equal to the Bogatyrev *et al.* (2015) temperatures of 280K and 800K, respectively, and a range of bulk flow velocities were employed. The boundary conditions employed in the simulations are summarized in table (4).

The simulations were conducted on a 1-dimensional computational mesh consisting of 30 grid points logarithmically distributed between the wall and the bulk. A grid sensitivity study showed that the wall heat flux and wall shear stress varied with less than 1% between a grid with 30 grid points and one with 100 grid points. The first grid point was located 10^{-7} m away from the wall, and the bulk node was located 10^{-3} m away from the wall. The results were insensitive to decreasing the first node distance to the wall.

To isolate the effect of non-zero composition gradients, simulations with and without diffusion were conducted. In the simulations without diffusion, the multicomponent diffusion coefficients were set to zero, $D_{ij} = 0 \forall i, j$.

4.3. Simulation results

In the simulations without diffusion, the mass-fraction profiles were constant throughout the boundary layer, and fluid properties varied only due to the varying temperature. In simulations including diffusion, however, non-constant mass-fraction profiles resulted to balance the thermophoretic diffusion by turbulent-diffusiophoretic diffusion, to maintain zero net diffusive transport. The resulting mass-fraction profiles are shown in figure (1), for the various bulk flow velocities (darker curve corresponds to higher velocity). Generally, the mass-fraction of CO_2 increased towards the wall while H_2 and N_2 mass-fractions decreased. Due to the fluid properties- (e.g. mass density and viscosity) composition dependency, the simulations predict a bulk flow velocity dependency in these.

In figures (2) and (3), respectively, the wall mass density and dynamic viscosity are shown as functions of the bulk flow velocity. It is seen that the failure to consider diffusion, resulted in underprediction of the fluid mass density and viscosity at the wall. Moreover, in the absence of diffusion, the mass density and viscosity are insensitive to the flow velocity since the wall temperature was fixed. However, due to their dependence on composition, they become flow velocity dependent when diffusion is considered. The near-wall enrichment of CO_2 , which is the densest fluid component, causes the fluid density

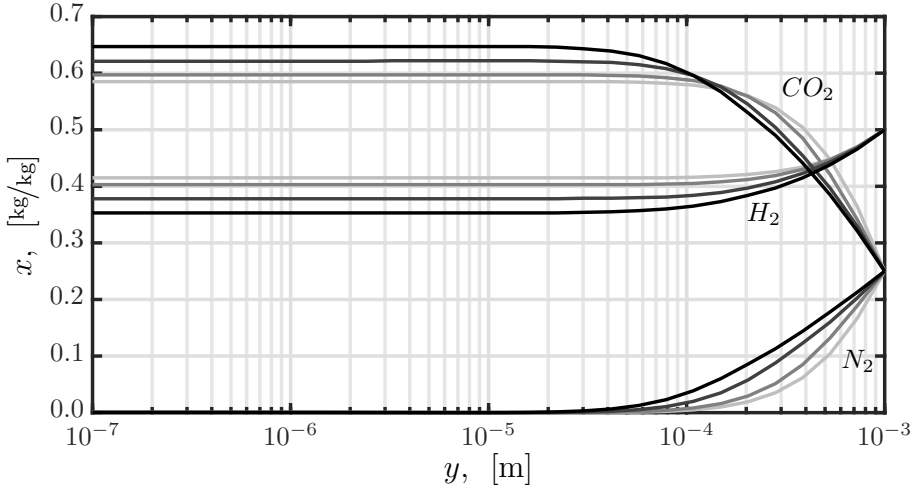


FIGURE 1. Calculated mass-fractions, x , plotted against wall distance, y , for the three species H_2 , N_2 , and CO_2 , for the bulk flow velocities 1 (light grey), 2, 5, and 10m/s (black).

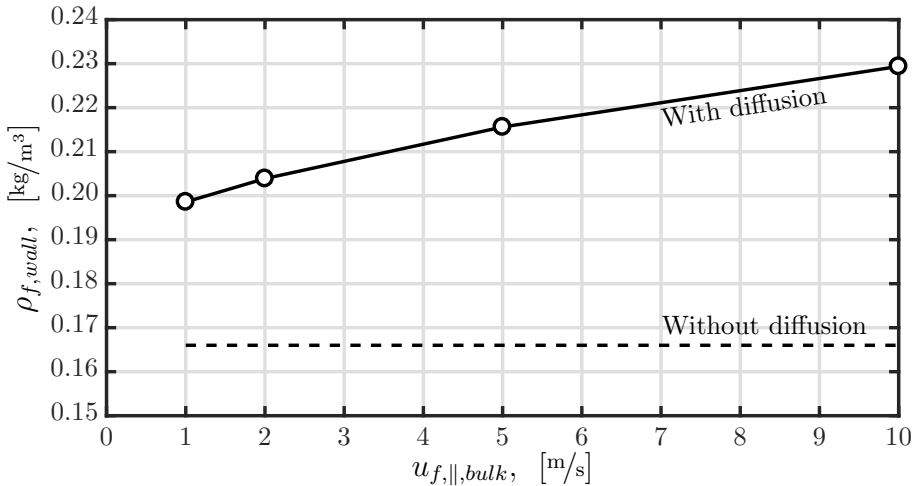


FIGURE 2. Calculated fluid mass density at the wall, $\rho_{f,wall}$, plotted against bulk flow velocity, $u_{f,||,bulk}$, with and without diffusion included.

to increase towards the wall. Since the enrichment increases with the flow velocity (see figure (1)), the mass density at the wall also increases with flow velocity.

In figure (4), the wall heat flux is shown as a function of the bulk flow velocity, for simulations with and without diffusion. Negative heat flux indicates that the heat flows from the fluid into the wall, and the magnitude of the wall heat flux generally increases with the bulk flow velocity, as expected, due to the increased efficiency of turbulent heat transport. The calculated wall heat flux was 18 and 8.6% lower with diffusion than without, in the $u_{f,||,bulk} = 1$ and 10m/s simulations, respectively. This was mainly due to the predicted diffusion-induced reduction of the fluid's thermal conductivity at the wall.

In figure (5), the wall shear stress is shown as a function of the bulk flow velocity, for simulations with and without diffusion. The wall shear stress increases with increasing

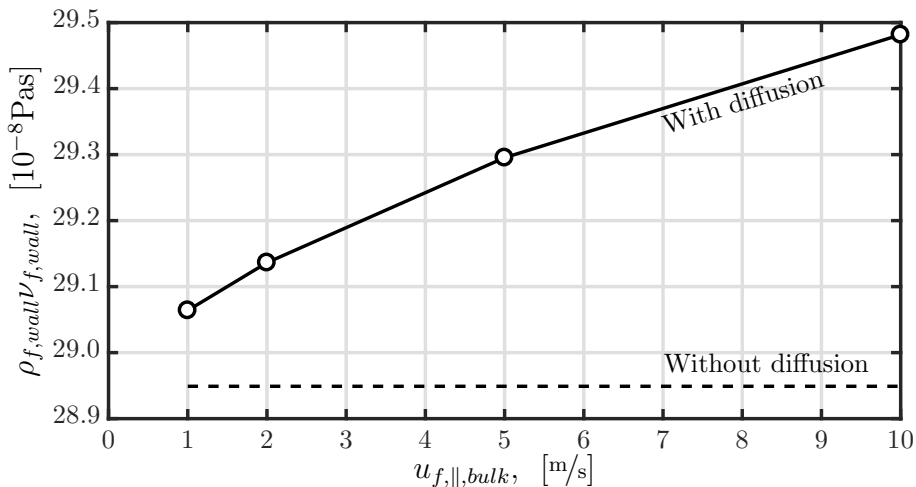


FIGURE 3. Calculated dynamic fluid viscosity at the wall, $\rho_{f,wall}\nu_{f,wall}$, plotted against bulk flow velocity, $u_{\parallel,bulk}$, with and without diffusion included.

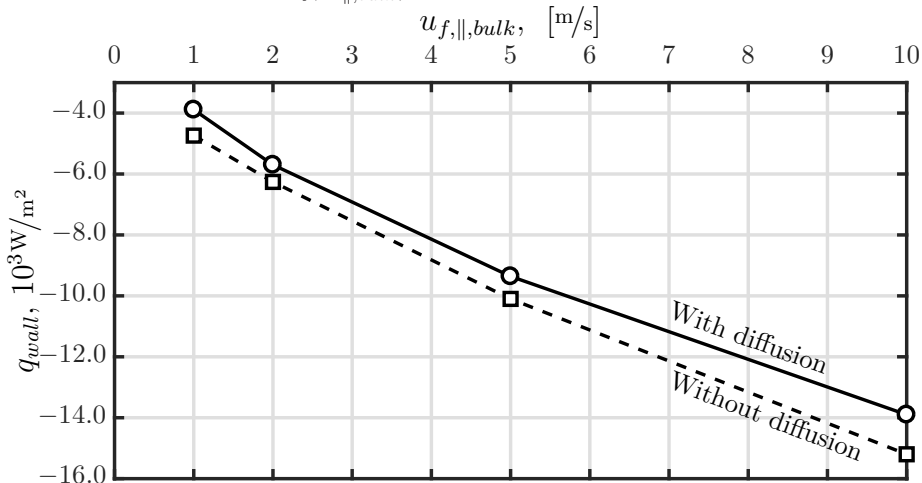


FIGURE 4. Calculated wall heat flux, q_{wall} , plotted against bulk flow velocity, $u_{\parallel,bulk}$, with and without diffusion included (negative heat flux indicates that heat is flowing from the fluid into the wall).

flow velocity, as expected, and the simulations predict that diffusion will increase the growth rate. The calculated wall shear stress was 4.7 and 12% higher with diffusion than without, in the $u_{f,\parallel,bulk} = 1$ and 10 m/s simulations, respectively. This was mainly due to the diffusion-induced increase in viscosity.

5. Conclusion

Employing mathematical modeling, it has been shown that the combined turbulent, diffusiophoretic and thermophoretic diffusion can have a considerable effect on composition profiles in the boundary-layer for inert, multicomponent fluids. This is of importance

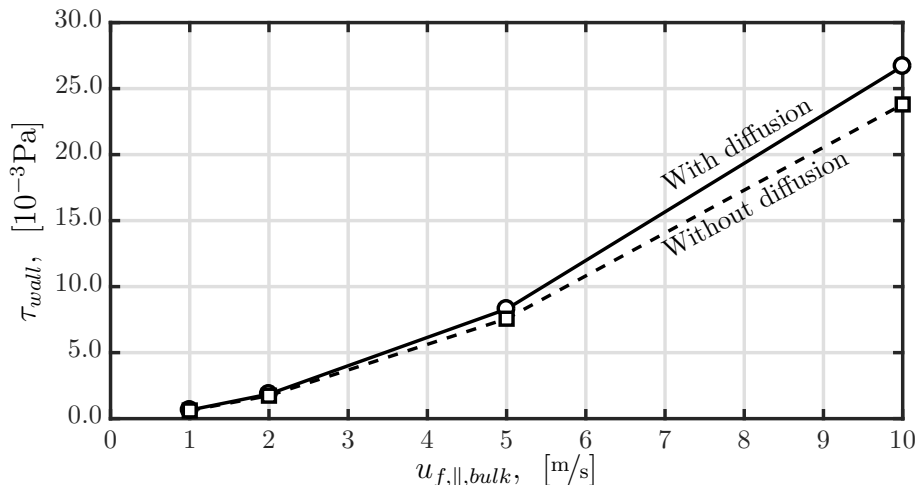


FIGURE 5. Calculated wall shear stress, τ_{wall} , plotted against bulk flow velocity, $u_{\parallel,bulk}$, with and without diffusion included.

for e.g. the interpretation of measurements relying on wall heat flux and/or wall shear stress data. Fluid properties derived from such measurements (e.g. viscosity or thermal conductivity) typically depend on the fluid composition, which may differ significantly between the bulk and the wall. Hence, failing to take diffusion into account may result in interpreted fluid properties that represent the bulk fluid inaccurately. Moreover, the effect of non-constant composition profiles may impact the design and mathematical modeling of flow systems sensitive to drag and/or heat exchange.

Mathematical proof was given to support the following statements for inert mixtures:

- Under isothermal conditions, in the absence of body forces:
 - Non-constant composition profiles requires that $-\nu_t^+/s_{c_t}$ is an eigenvalue of the matrix product $\mathbf{D}^+ \Gamma \Lambda$.
 - Non-zero compositional gradients at the wall requires that $\det(\Gamma) = 0$.
 - Ideal mixtures are not permitted to have non-zero compositional gradients at the wall.
- Under non-isothermal conditions, in the absence of body forces:
 - Non-constant composition profiles are required to counter thermophoresis.
 - For ideal mixtures, the thermophoretic driving force coefficients must obey $\sum_{j=1}^N z_j dT_{,j} = 0$.
- Under isothermal conditions influenced by gravitational/centrifugal body forces:
 - Non-constant composition profiles are required to balance barophoresis if the pure state mass density of one or more of the species differ from the fluid mass density.
 - Under laminar conditions, the segregation length is given by $|(RT)/(f_{\perp} \Delta M_m)|$ in diluted an binary mixtures.
 - Turbulence will reduce the segregation efficiency, hence increase the segregation length.

Gratitude goes to all the colleagues at the research group of flow technology at dept. Process technology, SINTEF Industry, in Trondheim, Norway. Without the vibrant research environment and fruitful discussions, this paper would not be. In particular, Roar

Meland and John C. Morud contributed with to-the-point comments and discussions and with reviewing the paper. The study was financed by SINTEF Industry and NTNU.

Appendix A. Dimensionless Variables

The model equations presented in this paper are presented in dimensionless form. Dimensionless variables are denoted by superscript $+$. When making the conservation equations dimensionless, typical wall unit scaling is employed. The subscript *wall* indicate property values at the wall. Selected scaled variables are given below.

The shear velocity is defined as

$$u_\tau = \sqrt{\tau_w / \rho_{f,wall}} , \quad (\text{A } 1)$$

the dimensionless wall distance is defined as

$$y^+ = y u_\tau / \nu_{f,wall} , \quad (\text{A } 2)$$

where y is the normal distance to the wall. $\nu_{f,wall} = \mu_{f,wall} / \rho_{f,wall}$ is the kinematic viscosity at the wall, the dimensionless fluid velocity is defined as

$$u_f^+ = u_f / u_\tau , \quad (\text{A } 3)$$

and the dimensionless mass flux is given by

$$j^+ = j / \rho_{f,wall} u_\tau . \quad (\text{A } 4)$$

Fluid properties are typically converted to wall units by scaling with the value at the wall, e.g.:

$$\text{mass density:} \quad \rho_f^+ = \rho_f / \rho_{f,wall} ; \quad (\text{A } 5)$$

$$\text{kinematic viscosity:} \quad \nu_f^+ = \nu_f / \nu_{f,wall} ; \quad (\text{A } 6)$$

$$\text{thermal conductivity:} \quad k_f^+ = k_f / k_{f,wall} . \quad (\text{A } 7)$$

The dimensionless, turbulent thermal conductivity is defined as

$$k_t^+ = \nu_t^+ \rho_f^+ c_{P,f}^+ (Pr_{wall} / Pr_t) , \quad (\text{A } 8)$$

and the dimensionless turbulent kinematic viscosity is modeled as (Johansen 1991)

$$\nu_{t,f}^+ = \begin{cases} (y^+ / 11.15)^3 & \text{for } y^+ < 3.0, \\ (y^+ / 11.4)^2 - 0.049774 & \text{for } 3.0 \leq y^+ \leq 52.108, \\ 0.4y^+ & \text{for } 52.108 < y^+. \end{cases} \quad (\text{A } 9)$$

Diffusivities are scaled by the fluid kinematic viscosity at the wall, e.g.

$$D_{ij}^+ = D_{ij} / \nu_{f,wall} . \quad (\text{A } 10)$$

The dimensionless temperature is given by

$$T^+ = T u_\tau \rho_{f,wall} c_{P,f,wall} / q_w - T_{wall}^{0+} , \quad (\text{A } 11)$$

where

$$T_{wall}^{0+} = T_{wall} u_\tau \rho_{f,wall} c_{P,wall} / q_{wall} , \quad (\text{A } 12)$$

and $q_{wall} = -k_f \partial_\perp T|_{wall}$ is the wall heat flux. The Prandtl number is given by

$$Pr = c_{P,f} \rho_f \nu_f / k_f . \quad (\text{A } 13)$$

Constant turbulent Prandtl and Schmidt numbers of $Pr_t = 0.85$ and $Sc_t = 0.7$, respectively, were employed in simulations.

REFERENCES

- ANDERSON, J. D., JR. 2006 *Hypersonic and High Temperature Gas Dynamics*. AIAA.
- BOGATYREV, A. F., MAKEENKOVA, O. A. & NEZOVTINA, M. A. 2015 Experimental study of thermal diffusion in multicomponent gaseous systems. *International Journal of Thermophysics* **36** (4), 633–647.
- DE GROOT, S. R. & MAZUR, P. 2011 *Non-Equilibrium Thermodynamics*. New York, USA: Dover Publications, Inc.
- DUNCAN, J. B. & TOOR, H. L. 1962 An experimental study of three component gas diffusion. *AIChE Journal* **8**.
- DYSON, P. & RANSING, R. 2005 Modelling of boundary layer at nanoscale. In *13th ACME conference: University of Sheffield*.
- DYSON, P., RANSING, R. S., WILLIAMS, P. M. & WILLIAMS, P. R. 2008 *Fluid Properties at Nano/Meso Scale: A Numerical Treatment*. Chichester, UK: John Wiley & Sons, Ltd.
- GIBBS, J. W. 1928 *The Collected Works of J. Willard Gibbs in Two Volumes*. Yale University Press.
- HIRSCHFELDER, J. O., CURTISS, C. F. & BIRD, R. B. 1964 *Molecular Theory Of Gases And Liquids*. Wiley.
- JOHANSEN, S. T. 1991 The deposition of particles on vertical walls. *International Journal of Multiphase Flow* **17** (3), 355–376.
- JOHNSEN, S. G., JOHANSEN, S. T. & WITTEGENS, B. 2015 A wall-function approach for direct precipitation/crystallization fouling in CFD modelling. In *Heat Exchanger Fouling and Cleaning XI - 2015*, arXiv: <https://arxiv.org/abs/1706.02931>.
- KJELSTRUP, S. & BEDEAUX, D. 2008 *Non-Equilibrium Thermodynamics of Heterogeneous Systems*. Singapore: World Scientific Publishing Co. Pte. Ltd.
- KOCHERGINSKY, NIKOLAI & GRUEBELE, MARTIN 2016 Mechanical approach to chemical transport. *Proceedings of the National Academy of Sciences* **113** (40), 11116–11121, arXiv: <http://www.pnas.org/content/113/40/11116.full.pdf>.
- KRISHNA, R. & WESSELINGH, J. A. 1997 The Maxwell-Stefan approach to mass transfer. *Chemical Engineering Science* **52** (6), 861 – 911.
- LINSTROM, P. J. & MALLARD, W. G., ed. 2018 *NIST Chemistry WebBook, NIST Standard Reference Database Number 69*. Gaithersburg MD, 20899: National Institute of Standards and Technology.
- MUCKENFUSS, C. 1973 Stefan-Maxwell relations for multicomponent diffusion and the chapman-enskog solution of the boltzmann equations. *The Journal of Chemical Physics* **59**.
- SCHULTE, A. M. 1980 SPE 9235: Compositional variations within a hydrocarbon column due to gravity. In *SPE Annual Technical Conference and Exhibition*. Dallas, Texas.
- SVEDBERG, T. 1927 The Svedberg - Nobel Lecture: The ultracentrifuge.
- TAYLOR, R. & KRISHNA, R. 1993 *Multicomponent Mass Transfer*. John Wiley & Sons, Inc.
- VAN DER VALK, F. 1963 Thermal diffusion in ternary mixtures: I. theory. *Physica* **29** (5), 417 – 426.